Mechanism of Inactivation Gating of Human T-Type (Low-Voltage Activated) Calcium Channels

Don E. Burgess,*† Oscar Crawford,* Brian P. Delisle,* and Jonathan Satin*
*Department of Physiology, University of Kentucky College of Medicine, Lexington, Kentucky 40536, and †Asbury College, Department of Physics, Wilmore, Kentucky 40390 USA

ABSTRACT Recovery from inactivation of T-type Ca channels is slow and saturates at moderate hyperpolarizing voltage steps compared with Na channels. To explore this unique kinetic pattern we measured gating and ionic currents in two closely related isoforms of T-type Ca channels. Gating current recovers from inactivation much faster than ionic current, and recovery from inactivation is much more voltage dependent for gating current than for ionic current. There is a lag in the onset of gating current recovery at −80 mV, but no lag is discernible at −120 mV. The delay in recovery from inactivation of ionic current is much more evident at all voltages. The time constant for the decay of off gating current is very similar to the time constant of deactivation of open channels (ionic tail current), and both are strongly voltage dependent over a wide voltage range. Apparently, the development of inactivation has little influence on the initial deactivation step. These results suggest that movement of gating charge occurs for inactivated states very quickly. In contrast, the transitions from inactivated to available states are orders of magnitude slower, not voltage dependent, and are rate limiting for ionic recovery. These findings support a deactivation-first path for T-type Ca channel recovery from inactivation. We have integrated these concepts into an eight-state kinetic model, which can account for the major characteristics of T-type Ca channel inactivation.

INTRODUCTION

The combination of a low-voltage activation range and a relatively slow deactivation rate (Huguenard, 1996) allows T-type Ca channels to function as a depolarizing current injector in the range of potentials corresponding to action potential threshold (Kozlov et al., 1999). With respect to pacemaking, for example, the kinetics of inactivation and recovery from inactivation of T-type Ca channels become critical determinants of cellular excitability (Huguenard and Prince, 1994; Coulter et al.,1989). Thus a quantitative description of T-type Ca channel kinetics is important for understanding the contribution of T-type Ca channels to excitability in neurons and cardiac myocytes. In a continuation of earlier work (Satin and Cribbs, 2000), we now measure gating current in two closely related T-type Ca channel isoforms (α1G and α1H) to determine how differences in ionic current recovery from inactivation are related to differences in certain gating transitions among inactivated states. The main point of this paper is to elucidate the gating processes underlying recovery from inactivation by exploring the kinetics and voltage dependence of gating current and ionic current.

Gating current measurements are essential to achieving a better understanding of the mechanisms underlying channel kinetics. Gating currents represent intramolecular motions of ion channels in response to changes in transmembrane potential. In contrast to ionic currents that only reflect the opening and closing of conducting channels, gating currents manifest transitions between nonconducting channel states. Central to this study, gating current measurements revealed transitions among inactivated states.

Evolutionarily, T-type Ca channels are thought to be intermediate between high-voltage activated Ca channels and Na channels (reviewed in Hille, 2001). Not surprisingly, T-type Ca and Na channels have some qualitatively similar gating kinetics. For example, the inactivation process itself is voltage independent. The apparent voltage dependence of macroscopic inactivation can be explained by the voltage dependence of the activating gating transitions (Aldrich et al., 1983; Chen and Hess, 1990; Droogmans and Nilius, 1989; Serrano et al. 1999). In parallel to Na channels, T-type channels appear to follow a deactivation-first route to recover from inactivation (Kuo and Bean, 1994; Satin and Cribbs, 2000; Kuo and Yang, 2001). The studies of Satin and Cribbs (2000) and Kuo et al. (2001) used macroscopic ionic current measurements to infer a deactivation-first pathway for recovery from inactivation (RFI). We now report our use of gating current measurements to provide further evidence for a deactivation-first route for RFI.

To quantitatively define T-type gating characteristics without contaminating currents, we used cloned channels expressed in heterologous expression systems. The T-type Ca channel family consists of three genes called α1G ($Ca_V3.1$), α1H ($Ca_V3.2$), and α1I ($Ca_V3.3$; nomenclature reviewed by Hille, 2001). Our initial studies of cloned, heterologously expressed α1G and α1H ionic currents demonstrated that the α1G and α1H ionic current characteristics were similar. However, α1G macroscopic inactivation and RFI kinetics are faster compared with α1H (Klockner et al., 1999; Satin and Cribbs, 2000).

Submitted August 10, 2001, and accepted for publication January 14, 2002.

Address reprint requests to address for correspondence Dr. Jonathan Satin, Department of Physiology, MS-508, University of Kentucky, College of Medicine Lexington, KY 40536-0298. Tel.: 859-323-5356; Fax: 859-323-1070; E-mail: jsatin1@uky.edu.

0006-3495/02/04/1894/13 $2.00

A central result of our present study is that gating charge movement for transitions between inactivated states are much faster than transitions from inactivated to available states. Furthermore, the transitions from inactivated to available states become rate limiting for ionic current RFI. Consequently, the ionic current RFI rate saturates for modest recovery potentials for this class of Ca channel. The time constants of deactivation and the decay of gating current arising from inactivated gating transitions are similar, and are voltage dependent, over a range where ionic current RFI is already saturated. Taken together, these results support a deactivation-first path for T-type Ca channel RFI. We put these ideas into the framework of a kinetic scheme. Our model captures the major features of our gating and ionic current measurements and quantifies our conceptual understanding of T-type Ca channel gating kinetics.

MATERIALS AND METHODS

Cell culture

α1H cDNA (Cribbs et al. 1998) was used to generate a stably-transfected HEK 293 cell line (Zhang et al. 2000). The α1G cell line (α1G-a; for nomenclature see Monteil et al., 2000b) was generously provided by Drs. Cribbs and Perez-Reyes (Perez-Reyes et al. 1998). Cells were incubated in DMEM, supplemented with10% fetal bovine serum, 100 U/ml penicillin, 100 mg/ml streptomycin, and 1 mg/mL G-418.

Electrophysiology

Cells were digested with 0.125% trypsin and replated 1–3 days before recording. Currents were recorded in the whole-cell clamp configuration. Culture media was replaced with the extracellular bath solution immediately before recording. Recordings were initiated 5 min after patch break to allow equilibration of the pipette solution with the cell interior. All recordings from α1G- and α1H-expressing cells were performed using identical ionic solutions and conditions. The pipette solution contained (in mM): 110 potassium gluconate, 40 CsCl, 1 $MgCl_2$, 3 EGTA, and 5 Hepes, pH 7.35 with CsOH. The bath consisted of (in mM): 140 NaCl, 2.5 $CaCl_2$, 5 CsCl, 2.5 KCl, 10 TEA-chloride, 1 $MgCl_2$, 5 glucose, and 5 Hepes, pH 7.4 with NaOH. All experiments were performed at room temperature (20–22°C). Patch electrodes were 1–2.5 MΩ using the above pipette solution. Cell capacitance was <20 pF. The series resistance (R_s) in the whole-cell configuration was <5 MΩ before R_s compensation. R_s was compensated >75% with the circuitry on the Axopatch 200 (Axon Instruments, Foster City, CA). Currents were low-pass filtered at 10 kHz and sampled at 100 kHz. Leak and capacity transients were subtracted with either P/6 (ionic current) or P/8 (ionic and gating current) protocols. Gating current protocols were performed with both P/8 and P/−8 to evaluate whether resolvable gating charge current moved in the range of potentials used for subtraction. No difference in gating or ionic current was observed for P/8 versus P/−8 protocols. In addition, execution of the P/8, P/−8 either before or after the test step yielded the same result. Therefore, even if a small amount of gating charge moved during our leak and capacity transient subtraction pulses, we could not detect any charge movement in the voltage range used for leak/capacity transient steps. Our electronics limited our resolution of fast gating currents to transitions slower than ~120 μs.

Stable-transfected HEK 293 cells sporadically failed to express T-type Ca current. These cells were used as controls to monitor endogenous currents. HEK 293 cells showed no detectable endogenous currents in response to the protocols used for this study (Fig. 1).

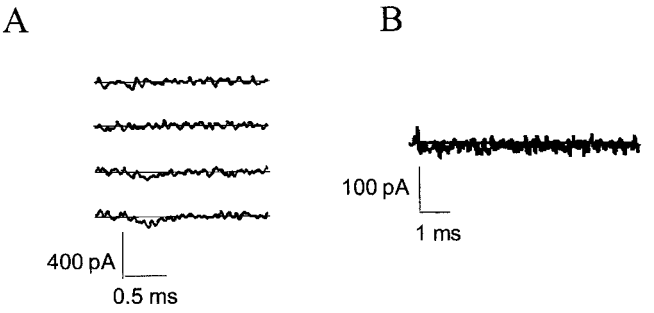

FIGURE 1 HEK 293 cell endogenous currents. (*A*) Recovery from inactivation protocol. Shown from top to bottom are recovery intervals of 1.3, 3, 100, and 10,000 ms; $V_{recovery} = -100$ mV (protocol the same as in Figs. 2 and 3). Note the absence of a detectable current. (*B*) Tail deactivation background. Current elicited by a voltage step from 0 mV to −180 mV.

Analysis

pClamp 6.04 and 8.02b programs (Axon Instruments) were used for data acquisition and analysis. Nonlinear curve fitting was performed with Origin v.4.1 (Microcal Software, Northampton, MA).

Voltage protocol details are provided in the text and in the figure legends. Gating currents were assessed by integrating the first 2–6 ms of the current time course. To assess recovery from inactivation, we measured current amplitude from single-exponential fits of tail current following a maximally activating depolarization. A 5-ms step to the Ca^{2+} current reversal potential (E_{rev}; ~+48 mV) coincided roughly with the time to peak of the inward current associated with maximally activating test potentials (>0 mV). The tail was recorded at −100 mV to amplify the inward current. With this protocol we could resolve small currents following brief recovery intervals, but the large tail currents following longer recovery intervals introduced increased error associated with the voltage drop across the series resistance (R_s). As a check for R_s error, we measured decay time constants for tail currents with different amplitudes (associated with different prepulse intervals) and found that the results deviated <10% for the same test potentials.

Modeling methods

Simulations were performed in MATLAB 5.3 (Math-Works, Natick, MA), using the built-in matrix exponential (expm) function call. When the voltage step was time dependent, we used the built-in ordinary differential equation (ODE) solvers to solve the kinetic equations. Because of the different time scales involved in the simulation, we used the stiff solver ode23s to numerically integrate the system of ordinary differential equations.

To find optimal model parameters, we used the optimization routines lsqcurvefit and lsqnonlin in the MATLAB Optimization Toolbox. We first fit the parameters using individual protocols. To obtain best-fit parameters, we minimized the least squares error from the following set of protocols: sustained depolarization, activation determined by the current peaks, steady-state inactivation of ionic current and gating charge, on-gating current traces measured during depolarization, recovery from inactivation of ionic current and gating charge, and deactivation of ionic current. The error for each protocol was normalized by the number of data points. By trial and error, we adjusted the weights given to each protocol to reflect the uncertainty in the corresponding data set and the difficulty of obtaining a good fit for that protocol.

There are several parameters in our model (see Fig. 7 below) that are poorly constrained by the data: $k_{-r'}$, $k_{-i'}$, $k_{i'}$, k_{-i}, and k_{I3Io}. Our experi-

TABLE 1 Voltage-independent rate constants

	αG	αH		1G	αH		αG	αH		αG	αH
k_r	0.0004	0.0002	k'_r	0.0013	0.0007	k_i	0.077	0.058	k_{C3O}	**0.84**	**0.42**
k_r	0.0012	0.0006	k'_{-r}	0.023	0.0034	k_{-i}	1.1×10^{-4}	8.0×10^{-5}			

Model parameters (ms^{-1}) were optimized for each isoform using data from only four experimental protocols: recovery from inactivation, steady-state inactivation, tail deactivation, and step depolarization. In addition, current traces of on gating current were used to further constrain the model parameters. The major differences between the two isoforms are related to the **C3-to-O** transition and the **I3-to-I2** transition, which are gating transitions.

mentally measured time constants indicate that deactivation governed by k_{OC3} is parallel to the first stage in recovery governed by k_{IoI3}. Thus, k_{I3Io} is similar to k_{C3O} because these two conformational changes appear to be related. To further constrain these parameters, we invoked microscopic reversibility (MR). We set $k_{i'} = k_i$; $k_{I3Io} = k_{C3O}$; $k_{-i'} = k_{-i}$ and we adjust $k_{-r'}$ and $k_{-i'}$ to satisfy MR in the first two boxes. Refer to Fig. 7 (below) for definition of the rate constants and refer to Tables 1 and 2 for a summary of the model parameters.

RESULTS

Gating current recovery precedes ionic current recovery from prolonged depolarization

We first measured RFI of ionic and gating current simultaneously in cells expressing the αG isoform. Fig. 2 *A* shows the voltage protocol we utilized. We first clamped the membrane potential at 0 mV for 10 s. We assumed that the channels were maximally inactivated at the end of this initial holding voltage (V_{hold}); this assumption is supported by the absence of ionic currents as ascertained by tail current analysis following prolonged depolarization (data not shown; see also Kuo and Yang, 2001). We then stepped the cell to hyperpolarized potentials for variable intervals. Next, to measure recovery of ON gating charge we stepped the membrane potential to E_{rev} for 5 ms. Finally, to ascertain recovery of ionic current we ended the voltage waveform by a step to −100 mV. Fig. 2, *B* and *C*, shows representative currents for the E_{rev} step and the step back to −100 mV for the αG isoform. Upon stepping to E_{rev} (~+48 mV), a brief transient outward current was evident, which we identified as ON gating current.

The transient outward current in Figs. 2 and 3 represents αG intra-membrane charge movement at E_{rev}. Fig. 2 *C* shows that for a 3-ms recovery interval (for $V_{rec} = -120$ mV) there is almost maximal charge movement but no resolvable ionic current. For recovery intervals less than 6 ms we could not detect ionic current by stepping back to −100 mV. It is obvious from the data that the time course of gating charge recovery is faster than that for ionic current. This experimental result supports the idea that the αG channel must deactivate before recovering from inactivation (Satin and Cribbs, 2000; Kuo and Yang, 2001) rather than recovering directly to the open state.

In contrast to the dynamics of the voltage-gated Na channel, the voltage dependence for the time course of αG channel ionic current RFI starts to saturate for recovery voltages negative to −80 mV. This saturation is evident in Fig. 2 where the amplitudes of the ionic tail currents in *C* for $V_{rec} = -120$ mV are comparable to those in *B* for $V_{rec} = -80$ mV.

αG channels recover more quickly from inactivation compared with αH (Satin and Cribbs, 2000). To explore the basis for this observation, we used the same voltage protocol to measure ionic current and gating charge recovery for the closely related αH isoform. Current traces for the αH isoform are shown in Fig. 3, *A* and *B*. Qualitatively, αH recovery from inactivation appears to be similar to that for αG. (Compare Fig. 3, *A* and *B*, with Fig. 2, *B* and *C*). Thus, as for the αG isoform, gating charge recovers before ionic current, and the voltage dependence of recovery of ionic current starts to saturate at voltages negative to −80 mV.

The RFI kinetics for the two isoforms are directly compared in Fig. 4. The top two panels represent recovery of ionic current; the lower two panels represent recovery of gating charge. The symbols represent pooled data whereas the smooth lines are from simulations based on the eight-state model discussed below (Fig. 7) and detailed in the Appendix. As in the representative data, the pooled data show that 1) gating charge recovers before ionic current and 2) ionic current recovery saturates at −100 mV. The delay

TABLE 2 Voltage-dependent rate constants

Gating charge parameters			Amplitudes					
	αG	αH		αG	αH		αG	αH
Q_1	1.55	1.82	K_{C1C2}	2.50	1.6	K_{I1I2}	0.043	0.032
Q_2	3.96	4.50	K_{C2C1}	0.36	0.032	K_{I2I1}	0.0011	0.0004
Q_3	0.82	0.70	K_{C2C3}	29.0	41	K_{I2I3}	0.71	0.25
δ_1	0.80	0.72	K_{C3C2}	0.054	0.027	**K_{I3I2}**	**3.3×10^{-5}**	**1.1×10^{-6}**
δ_2	0.26	0.31	K_{OC3}	0.014	0.015			

See Table 1.

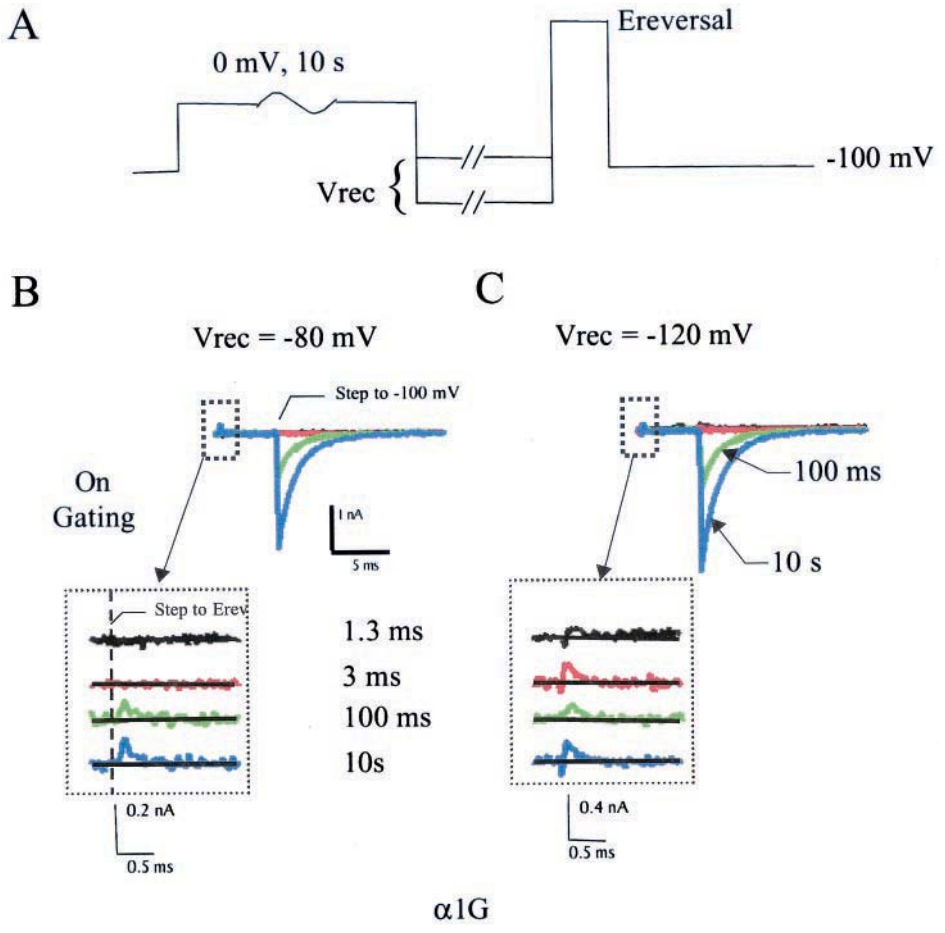

FIGURE 2 Recovery from inactivation protocol for the α1G isoform of the T-type calcium channel. (*A*) Recovery from inactivation voltage protocol. Cells were held at a membrane potential of 0 mV to inactivate the channels. Then, the cells were hyperpolarized to V_{rec} for time intervals ranging from 1.3 ms to 10 s, followed by a step to E_{rev} to measure the ON gating current. Finally, tail currents were elicited by stepping back to −100mV. The amplitudes of the tail currents were used as a measure of recovery from inactivation. (E_{rev} was determined for each cell with a separate protocol consisting of steps of a sustained depolarization in 2-mV increments around predicted E_{rev}.) (*B*) Representative currents beginning 0.2 ms before the step to E_{rev} following recovery intervals of 1.3 (*black*), 3 (*red*), 100 (*green*), and 10,000 (*blue*) ms. The initial outward current upon the step to E_{rev} is on gating current (I_{Qon}). The inward currents are ionic tail currents. Recovery potential = −80 mV. (*C*) Same as *B* except recovery potential = −120 mV. For the recovery interval of 3 ms almost all of the gating current has recovered with no ionic current present. That gating current recovery precedes ionic current indicates that the channel must deactivate to recover from inactivation. Note that compared to $V_{recovery} = -80$, the ionic current recovery time course is similar, but gating current recovers faster for $V_{recovery} = -120$ than $V_{rec} = -80$ mV.

in gating charge recovery is strongly voltage dependent. For $V_{rec} = -80$ mV there is a noticeable lag in the onset of gating current recovery, and for V_{rec} of −120 mV the lag is virtually undetectable. The lag in recovery from inactivation is larger for ionic current (Fig. 4, *A* and *B*) than for gating current (Fig. 4, *C* and *D*). Close examination of ionic recovery intervals less than 100 ms consistently reveals faster recovery with more hyperpolarized recovery potentials, revealing a voltage dependence for the delay in recovery from inactivation for ionic current (Figs 4, *A* and *B*).

The pattern of α1H recovery of gating charge from inactivation is similar to α1G (compare Fig. 4, *C* and *D*). At hyperpolarizing potentials negative to −120 mV the recovery for ON gating charge approaches a rapid rate that surpasses the limit of our resolution. The slower recovery of inactivation of α1H is apparent for more depolarized recovery potentials. For $V_{rec} = -80$ mV the half-time for on gating recovery is ~20 ms for α1G (Fig. 4 *C*), in contrast to 100–200 ms for α1H (Fig. 4 *D*). This is consistent with our prediction that the slower recovery kinetics for α1H is associated with the voltage-dependent deactivation gating kinetics of this isoform (Satin and Cribbs, 2000).

The delay in recovery from inactivation is related to the voltage dependence of deactivation gating charge movement

In Na channels the delay of recovery from inactivation is related to deactivation (Groome et al., 1999). To test

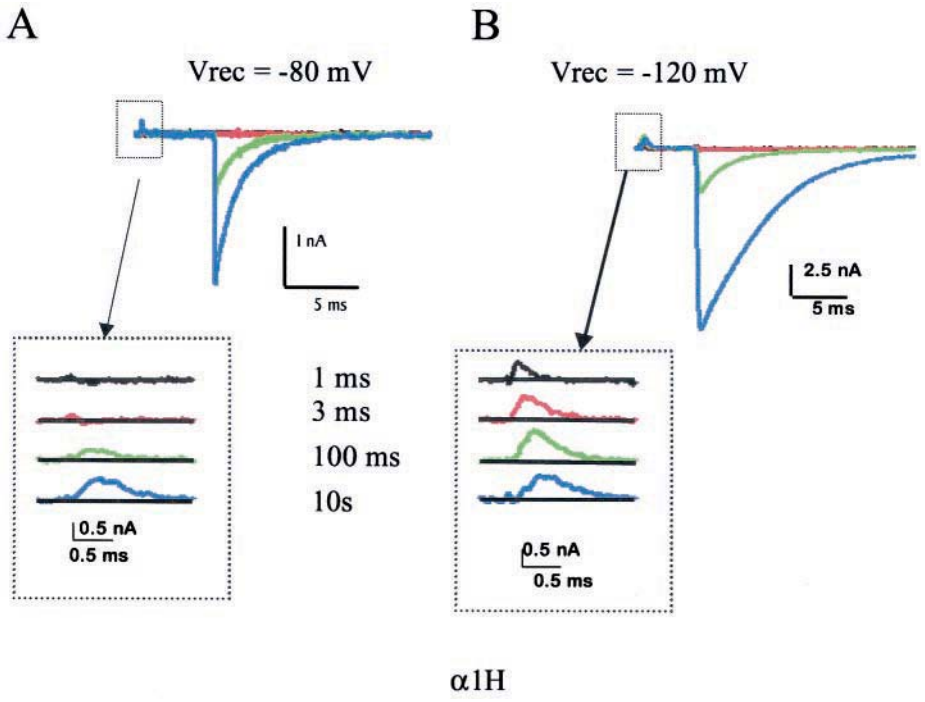

FIGURE 3 Recovery from inactivation for the α1H isoform of the T-type calcium channel. The voltage protocol is identical to the one displayed in Fig. 1 *A*. (*A* and *B*) Representative current traces (gating and ionic) for $V_{rec} = -80$ (*A*) and -120 mV (*B*), respectively. Similar to the α1G isoform, gating charge recovers before ionic current for a given V_{rec}.

whether the delay in ionic current recovery from inactivation for T-type Ca^{2+} channels is similarly related to channel deactivation, we compared gating charge movement from maximally inactivated channels to ionic current deactivation from the channel open state. To maximally inactivate channels we prepulsed the cells to 0 mV for 10 s. To study the kinetics of gating charge movement between inactivated states, we then performed a 10-ms test step back to various hyperpolarized potentials. Gating current is detectable for values of V_{test} negative to -100 mV (Fig. 5 *A*). The transient inward current that is measured at hyperpolarized potentials represents inactivated state off gating current (I_{Qoff}). The rate of I_{Qoff} decay is plotted (filled squares) in Fig. 5, *C* (α1G) and *D* (α1H). Interestingly, the rate of I_{Qoff} decay is similar to the rate of deactivation of ionic current (Fig. 5 *B*). Deactivation time constants were obtained in the same cell by measuring tail currents to given test potentials preceded by a 10-ms depolarization prepulse. These deactivation time constants are also plotted in Fig. 5, *C* and *D* (open triangles). The classical interpretation of indistinguishable gating and deactivation time constants is that the initial step in channel deactivation is independent of the inactivation process (Patlak, 1991). Although the kinetics of deactivation and off gating current appear to be similar, both processes are much faster than the delays in RFI that we measured (Fig. 4). Thus, the time course of off gating current occurs before ionic recovery can proceed. This experimental result indicates that the channels must deactivate before they can significantly recover from inactivation.

I_{Qoff} is not resurgent ionic current

As a test of our hypothesis that what we call OFF gating current is not a resurgent ionic current, we attempted to block I_{Qoff} with Ni^{2+}. At -30 mV, Ni^{2+} blocks ionic current through α1H and α1G with IC_{50} values of $\sim$10 μM and $\sim$200 μM, respectively (Lee et al., 1999). Ni^{2+} blockade of Ca^{2+} current is voltage dependent with stronger blockade produced at more hyperpolarized potentials (Lee et al., 1999). Ni^{2+} concentrations $>$200 μM would thus block ionic current but would have no effect on I_{Qoff}. Therefore, we tested whether 300-1000 μM Ni^{2+} selectively altered the deactivation amplitude and rate of ionic current versus I_{Qoff} in the same cells. For both α1G and α1H, Ni^{2+} reduced ionic current amplitude and altered the time course of decay of ionic current. However, Ni^{2+} had no effect on I_{Qoff} (Fig. 6 *A*) or OFF gating charge (Fig. 6 *C*). Ni^{2+} speeded the ionic current decay time course (Fig. 6 *D*) similar to that observed previously (Lee et al., 1999). However, Ni^{2+} had no effect on the I_{Qoff} decay rate (Fig. 6 *D*). Therefore, we conclude that I_{Qoff} is not resurgent ionic current.

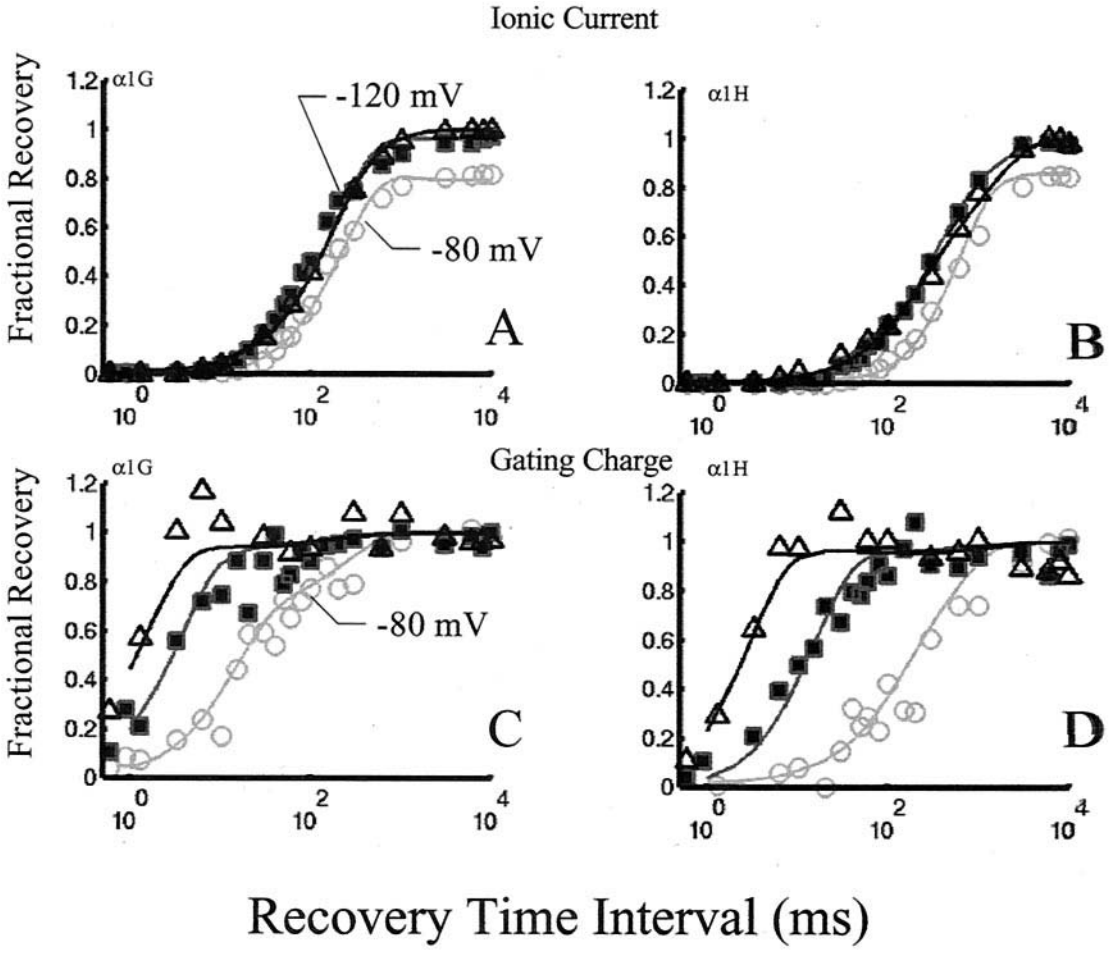

FIGURE 4 Recovery from inactivation of immobilized gating charge versus ionic current. (*A* and *B*) A comparison of the recovery of ionic current for α1G (*A*) and α1H (*B*). Curves are shown for $V_{rec} = -80$ (○), -100 (■), and -120 mV (△). The symbols are pooled experimental data, and the smooth lines are simulations based on the kinetic scheme shown below in Fig. 7. In comparison to the Na channel, the voltage dependence for the time course of the recovery of ionic current saturates early at voltages slightly more negative than -80 mV. (*C* and *D*) A comparison of the recovery of gating charge for α1G (*C*) and α1H (*D*). Gating charge recovers before ionic current for both isoforms. Note the strong voltage dependence for the delay in the recovery of gating charge and the overall time course of gating charge recovery from inactivation. This protocol reveals the largest single difference between the two T-type Ca channel isoforms under study. The α1H isoform recovers more slowly than the α1G isoform.

Model simulations predict mechanism for α1G versus α1H isoform functional differences

Quantitative models of channel gating are useful for inferring mechanisms of channel function. We have shown that α1G and α1H have indistinguishable voltage dependencies of ionic current activation and inactivation but distinct recovery from inactivation profiles. To help interpret these results we developed an eight-state Markovian model (Fig. 7).

We constrained the model with ionic and gating current data for the two T-type Ca channel isoforms. The overall kinetic scheme follows standard voltage-gated channel models: the vertical C-to-I transitions (which represent binding and unbinding of the inactivating particle) are assumed to be voltage independent, whereas the horizontal C-to-C, and I-to-I transitions (activation/deactivation gating transitions) are voltage dependent. We modeled the O-to-C transition as a voltage-dependent rate, because tail deactivation rate data do not exhibit a voltage-independent region for large hyperpolarizations (cf. Serrano et al., 1999). In contrast, we modeled the opening step, C to O, as a voltage-independent transition because the time to peak for large depolarizations reaches a nearly constant rate over a broad range of voltages (Chen and Hess, 1990). As for the Na channel, the voltage dependence of the inactivation time constant of T-type Ca channels is associated with activation gating transitions (Aldrich et al., 1983). For large depolarizations, the decay of ionic current saturates at a voltage-independent rate (k_i), which is associated with the binding of the inactivation gate. Details of the model are given in the Appendix. The scheme shown in Fig. 7 can accurately describe many features of the experimental data, including

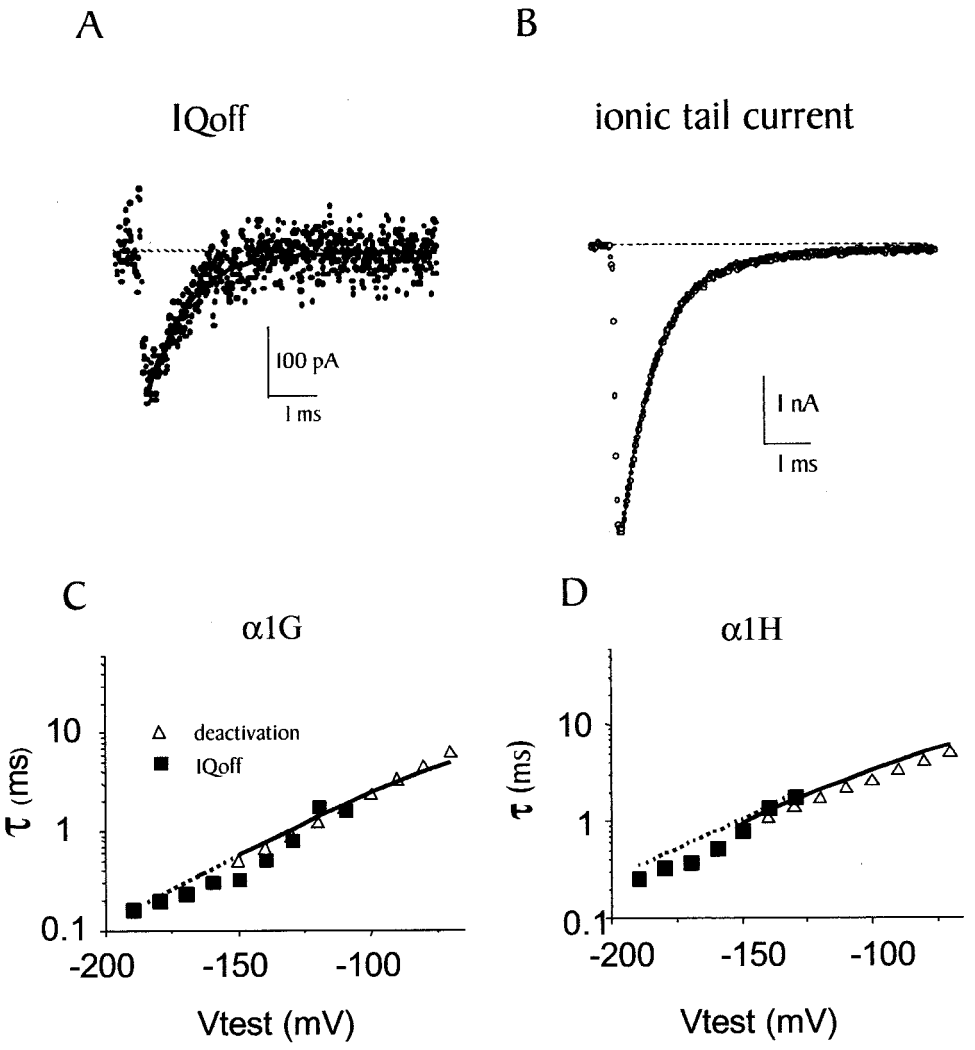

FIGURE 5 The decay rate of off gating current (I_{Qoff}) is not different from the decay rate of ionic tail current. (*A*) Inactivated-state off gating current (I_{Qoff}). Representative α1G current measured following a 10.8-s depolarization to 0 mV with a test step to −130 mV. The smooth line is a single-exponential fit with τ = 0.77 ms and amplitude = 211 pA. (*B*) Ionic tail current from the same cell as *A*. In contrast to measurement of I_{Qoff}, the prepulse duration to 0 mV was shortened from 10.8 s to 10 ms to measure deactivating ionic current. The smooth line is a single-exponential fit with τ = 0.87 ms and amplitude = 4.4 nA. (*C* and *D*) The time constant, τ, for the decay of I_{Qoff} (■) is plotted as a function of V_{test} for α1G (*C*) and for α1H (*D*). On the same axes, τ for deactivation of ionic current (△) is also plotted. The tight correspondence between the rate of deactivation and the decay of I_{Qoff} indicates that the rate of deactivation of the channel is relatively independent of inactivation. The solid lines (τ deactivation) and dashed lines (τ I_{Qoff}) are output of the eight-state model described below.

both ionic current measurements and gating charge measurements obtained over a voltage range from −190 mV to +50 mV. The model parameters (Tables 1 and 2) closely fit the data from RFI (Fig. 4, solid lines), ionic current deactivation time course (Fig. 5, solid lines), and I_{Qoff} time course (Fig. 5, dashed lines) measurements.

Fig. 8 compares the predictions of this model to data for OFF gating current. I_{Qoff} was elicited by a 10-s V_{hold} at 0 mV followed by hyperpolarized voltage steps ranging from −190 to −130 mV. The smooth lines are the model predictions superimposed on the experimental data. Because of the fast gating dynamics involved, we modeled the voltage step as having a rising phase determined by a fixed electronic time constant (see Appendix). The model predicts the relative normalization and the decay of the OFF gating current, although the rising phase is fit less effectively.

Fig. 9, *A* and *B*, are simulations of ionic currents obtained using sustained depolarization for both of the T-type Ca channel isoforms. The smooth lines superimposed over experimental data are simulations carried out using the kinetic scheme shown in Fig. 7. As shown by the figure, the model captures both the time course and the voltage dependence of the ionic currents. We measured peak inward currents elicited by a sustained depolarization to obtain the voltage dependence of activation (Cribbs et al., 2001). Fig. 9, *C* and *D*, compare modeled results (solid line) with experimental

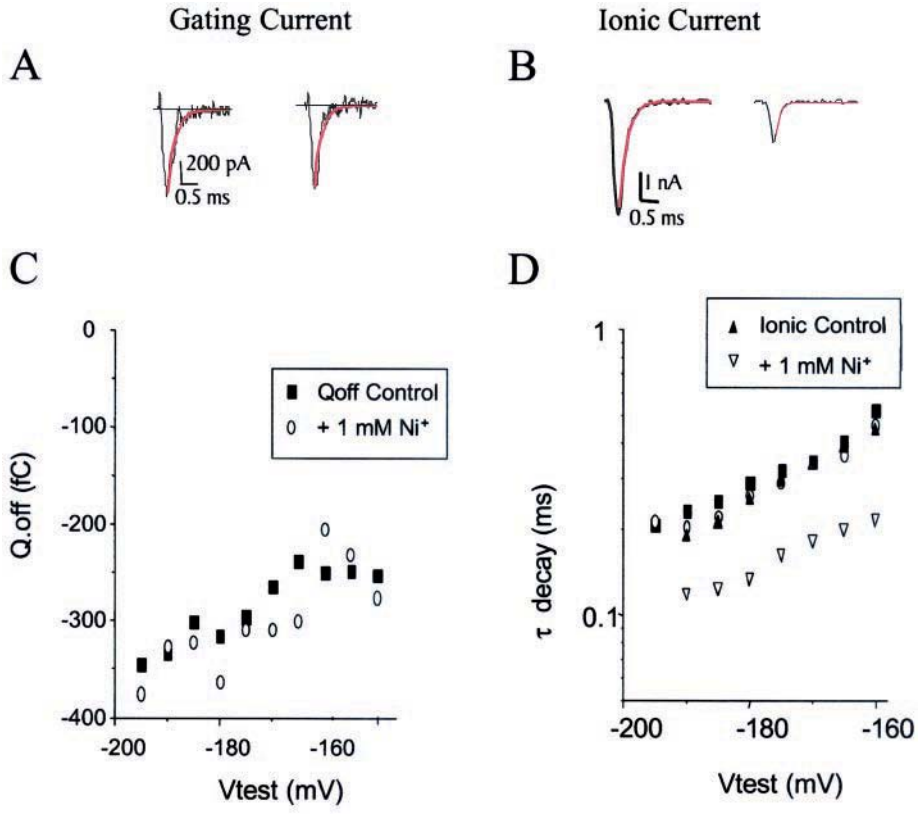

FIGURE 6 I_{Qoff} is not a resurgent ionic current. The 1 mM nickel has no effect on either amplitude of gating charge or decay of gating current, but Ni^{2+} blocks ionic current and speeds apparent deactivation rate. A representative α1G cell is shown. (*A*) Gating current, I_{Qoff}, elicited by a step from 0 mV (10.8 s) to −190 mV in control and 1 mM Ni^{2+}. Smooth line is a single-exponential fit of the decay of the gating current with τ = 0.23 and 0.20 ms and amplitude = 768 and 772 pA for control and 1 mM Ni^{2+}, respectively. (*B*) Ionic current deactivation elicited by a step from 0 mV (25 ms) to −190 mV in control and 1 mM Ni^{2+}. The 1 mM Ni^{2+} decreased ionic current amplitude ~75% for V = −190 mV. The smooth curve is a single-exponential fit of the deactivating current with τ = 0.19 and 0.13 ms and amplitude = 4.2 and 1.2 nA, for control and 1 mM Ni^{2+}, respectively. (*C*) Gating charge *Q* (the integral of gating current) is unaffected by 1 mM Ni^{2+}. ■, control; ○, 1 mM Ni^{2+}. (*D*) Time constant for decay of ionic current (▽ and ▲) and gating current (■ and ○). The 1 mM Ni^{2+} has no effect on gating current decay but speeds decay of ionic current. ▽, ionic current + 1mM Ni^{2+}; ▲, ionic current, control; ○, gating current + 1 mM Ni^{2+}; ■, gating current, control. Ni^{2+}-induced decrease of τ_{decay} is expected from accumulation of voltage-dependent Ni^{2+} blockade at large negative potentials superimposed on voltage-dependent deactivation. Though Ni^{2+} does not completely block ionic current, it serves as a probe to distinguish between ionic and gating current.

data (symbols) for activation for α1G and α1H, respectively. Fig. 10 shows deactivation of T-type Ca^{2+} current elicited by a prepulse to 0 mV for 5 ms, followed by a test potential ranging from −60 to −160 mV. The solid lines are from simulations based upon the kinetic scheme shown in Fig. 7, which include both ionic and gating currents. The expanded portion of each curve displays the outward gating current generated during the prepulse to 0 mV. For all protocols tested, the data show that the model simulations closely resemble the time course and voltage dependence of α1G and α1H ionic and gating currents.

DISCUSSION

This is the first study to measure gating currents from cloned α1G ($Ca_V3.1$) and α1H ($Ca_V3.2$) T-type Ca channels. Our data show that T-type Ca channel inactivation resembles Na channel inactivation in that deactivation precedes recovery from inactivation; however, there are significant quantitative differences between T-type Ca and Na channels. For example, inactivation is much slower in T-type Ca channels.

The similarities of T-type and Na channel kinetics may stem from the well known topographical homology between Ca and Na channels (Hille, 2001; Catterall, 1998). Unfortunately, unlike the situation for Na channels the detailed molecular basis of T-type inactivation is not known. Recent work shows that the IIIS6 transmembrane domain contributes to the rapid inactivation of α1G (Marksteiner et al., 2001), and the amino terminus of the cytosolic carboxy tail also contributes to T-type fast inactivation (Staes et al., 2001). Interestingly the IIIS6 domain also contributes to Na

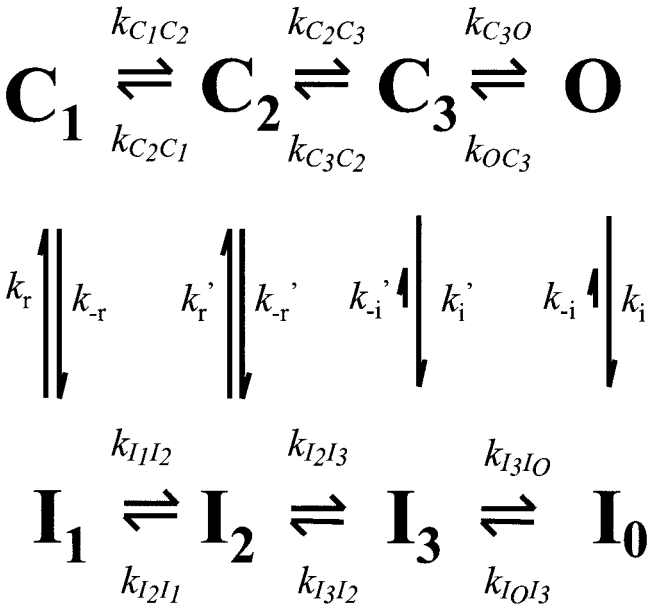

FIGURE 7 A kinetic scheme for gating of low-voltage activated Ca channels. We used a Markov model to simulate the experimental results of our voltage-clamp recordings. The rate constants for recovery from inactivation are voltage independent. All of the rate constants on the top and bottom rows of the model, except for k_{C3O} and k_{I3O}, have a voltage dependence. For resting (or hyperpolarized) membrane potentials, the most probable configuration is shifted to the left where an equilibrium is established between the I_1 and C_1 states. For large depolarizations, the voltage dependence of the rate constants drives the model toward the inactivated I_O state. In moving toward this equilibrium configuration, a certain portion of the channel proteins will pass through the open state O. Measurements of ionic current give a direct measure of the population of this open state.

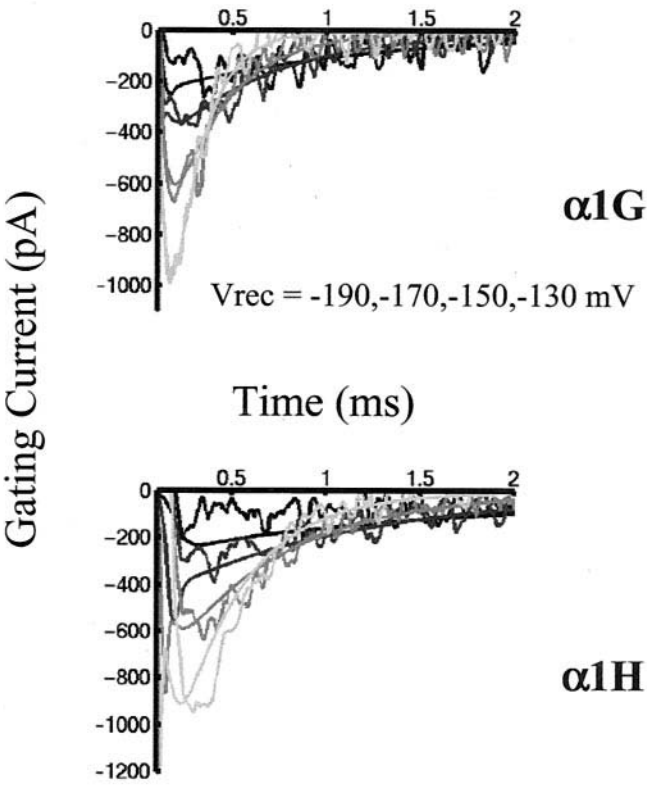

FIGURE 8 Prediction of off gating current. (*Top*) α1G; (*Bottom*) α1H. The smooth lines are from model simulations. The off gating current data are for $V_{recovery} = -190, -170, -150$, and -130 mV. These hyperpolarized voltage steps were preceded by a 10-s holding potential of 0 mV. This figure is a prediction because the model parameters were determined with data from other protocols.

channel fast inactivation (Yarov-Yarovoy et al., 2001). For simplicity of discussion, we suggest that the Na channel ball-and-chain conceptual model can be helpful in explaining our results.

We provide evidence that T-type channels recover from inactivation by first deactivating (present study; Satin and Cribbs, 2000; Kuo and Yang, 2001). Namely, the time course of recovery of gating charge was found to be faster than the recovery of ionic current. Again, this appears to be a conserved feature among different T-type Ca channel isoforms (α1G and α1H, this study) as well as Na channels (Kuo and Bean, 1994). Although qualitative parallels to Na channel gating schemes are apparent, the rates of RFI for saturating potentials are slower for T-type Ca channels than Na channels. Kuo and Bean (1994) for Na channels reported recovery rates of $\sim$4 ms^{-1} for potentials near -200 mV. In contrast, we find that the recovery rate constant (k_r) for T-type channels is 10,000 fold slower. This slower rate of RFI appears to be associated with tighter binding of the inactivating gating particle. Because T-type Ca channels deactivate before recovery from inactivation, the rate of recovery from inactivation may result from a slow rate of dissociation of the inactivating gating particle. Accordingly, the rate of RFI saturates at modest recovery potentials for T-type Ca channels (~ -90 mV) compared with Na channels (~ -200 mV).

The strong correspondence between current deactivation and the decay of OFF gating current (I_{Qoff}) indicate that the O-C_3 and I_O-I_3 transitions are likely to involve very similar conformational changes and that the kinetics of the conformational change are not strongly affected by the attachment of the inactivating peptide domain. Physically, this similarity in the kinetics of I_{Qoff} (which flows during deactivation with the ball attached) and ionic current deactivation (where the inactivating particle is dissociated) suggest that the binding of the inactivating ball has little effect on the initial deactivation steps of the channel. Similar correspondence has been noted in Na channels (Kuo and Bean, 1994; Groome et al., 1999). Also, microscopic reversibility (MR) in our gating model is consistent with the concept that the binding affinity of the ball is unaffected by the first deactivation step.

Isoform diversity

While the two T-type channel isoforms under study appear to have very similar binding rates for the inactivation ball,

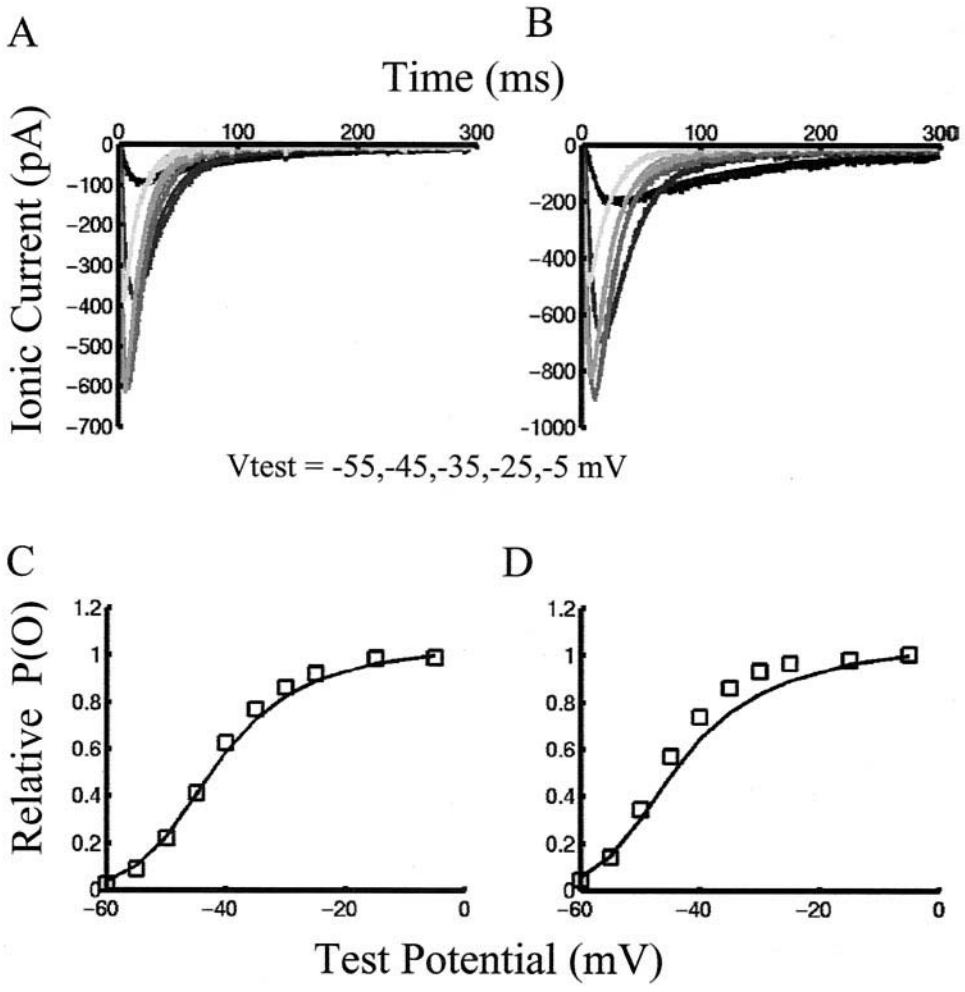

FIGURE 9 Sustained depolarization and activation. (*A* and *B*) Ionic current traces for sustained depolarizations; (*C* and *D*) Activation curves measured from the ionic current peaks. The smooth lines are simulations done with the kinetic scheme shown in Fig. 7. (*A* and *C*) Results for the α1G isoform; (*B* and *D*) Results for the α1H isoform. The symbols are from a representative cell, and the solid line is calculated from model simulations.

the isoforms appear to differ mainly in their rates of activation/deactivation gating. Overall, α1H ionic current RFI is slower than that for α1G. We previously showed that this is a consequence of the relative proportion of channels recovering with fast versus slow ionic current recovery time constants rather than differences in their recovery rates themselves (Satin and Cribbs, 2000). Our present modeling studies quantitatively support our earlier contention that the explanation for these differences in RFI rests in slower deactivation gating (I-I) transitions in α1H, compared with α1G, rather than differences in the dissociation rate of the inactivating ball (the I-C recovery transitions).

Our kinetic scheme shares qualitative features in common with earlier T-type Ca channel gating models (Chen and Hess, 1990; Droogmans and Nilius, 1989; Serrano et al., 1999). However, we do not assume that the gating can occur via four independent gating steps. With our current knowledge of the structure of the Na and Ca family of voltage-controlled channels, the assumption of four-fold symmetry becomes untenable. For example, the number of charges is not conserved among the S4 α-helices in the four different domains of T-type Ca channels (Perez-Reyes et al., 1998; Cribbs et al., 1998); in parallel, the homologous domains of the Na channel function unequally during gating (Cha et al., 1999). The lack of four-fold symmetry leads to additional rate constants and parameters. Rather than represent a transition corresponding to the movement of each S4 voltage sensor, we reduced the number of constants by using only the number of conformational states necessary to reproduce our experimental data.

In our model, transitions between closed and inactivated states are voltage independent, as is the open-to-inactivated state transition. These model transitions are thought to reflect the physical binding and unbinding of the inactivation ball, which seems to occur largely outside the electrical field of the membrane. This lack of voltage dependence is supported by the saturating value for the inactivation time

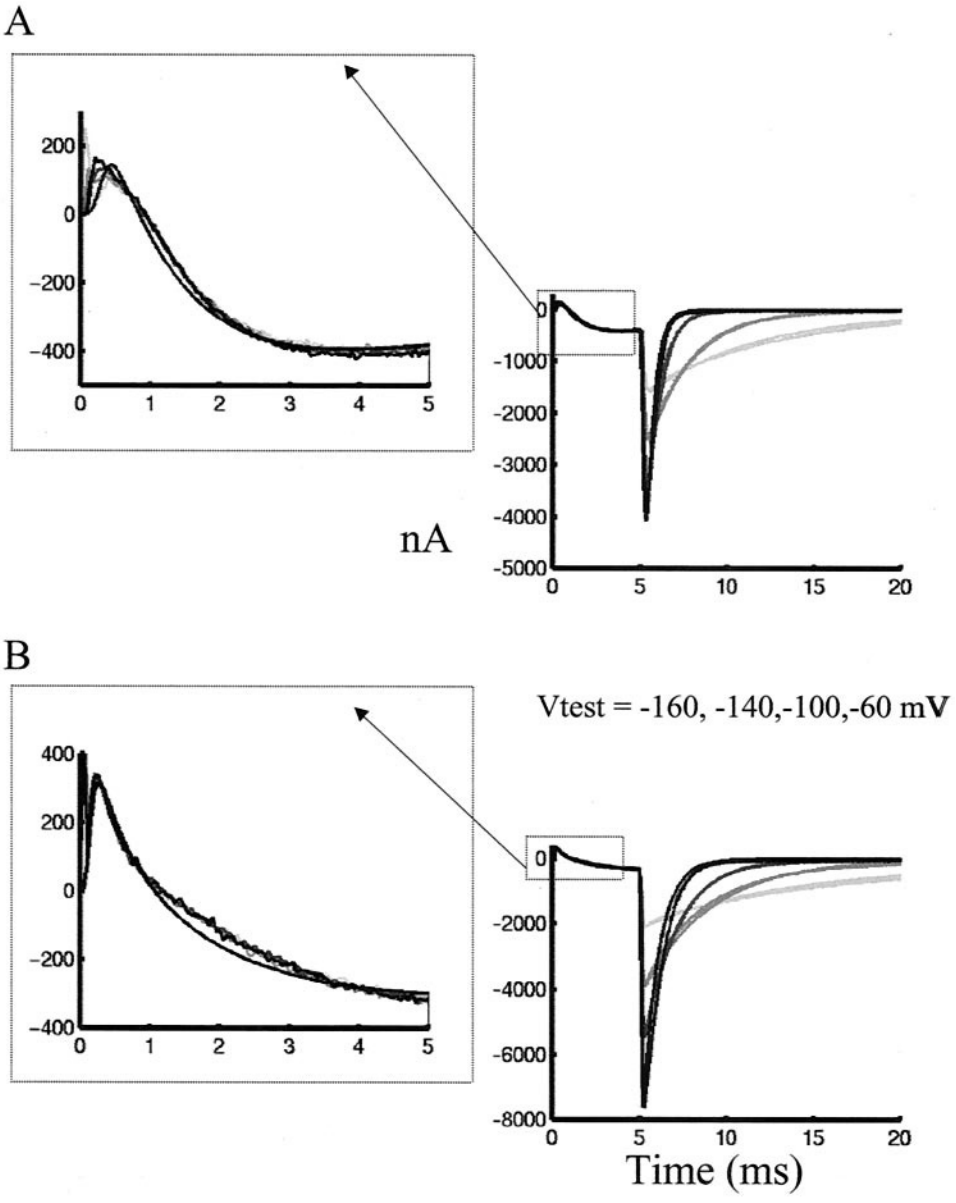

FIGURE 10 Deactivation tail currents: data and model predictions. (*A*) α1G; (*B*) α1H. The cell was clamped to a potential of −100 mV for 10 s followed by a step to 0 mV for 5 ms. Ionic tail currents were elicited by a step back to test potentials ranging from −60 mV to −160 mV. The enlarged portion of each figure shows the outward on gating current generated during the step to 0 mV. The smooth lines are simulations done with the kinetic scheme shown in Fig. 7.

constant of ionic current following a prolonged depolarization. As we showed recently (Satin and Cribbs, 2000), this parameter is not significantly different between α1G and α1H isoforms. Our findings describing the voltage independence of the inactivation reaction are in agreement with native T-type ionic current studies (Chen and Hess, 1990) and a previous study of heterologously expressed α1G channels (Serrano et al., 1999).

The gating scheme shown in Fig. 7 has three loops. We define box 1 as C1-C2-I2-I1, box 2 as C2-C3-I3-I2, and box 3 as C3-O-Io-I3. Our model satisfies microscopic reversibility (MR) for all three boxes. Pragmatically, MR is useful because it constrains parameters. MR imposes a very small, but finite return of channels from I_O to O (constituting a resurgent current; Raman and Bean, 1997). However, our value for k_{-i} predicts a small-amplitude resurgent current compared with the amplitude of what we call I_{Qoff}. For the experimental conditions shown in Fig. 6, the model predicts a resurgent current of 156 pA, which is ~20% of the measured gating current amplitude of 768 pA. Therefore, we predict that we cannot experimentally measure resurgent current because

the much larger gating current component is predicted to mask resurgent current.

Isoform-specific function: correlation with amino acid divergence

The primary amino acid sequences of α1G and α1H are 57% conserved at the amino acid level (Perez-Reyes et al., 1998; Cribbs et al., 1998). Most of the divergence is restricted to the large extracellular loops between S5 and S6, the large cytoplasmic loops between homogenous repeats I and II, II and III, and the N- and C-termini. The amino side of the C-terminus is known to be important for fast inactivation (Staes et al., 2001). A sequence of 23 amino acids in this C-terminal region are highly negatively charged and may serve as binding site for a putative peptide ball. Additional channel variability arises from alternative splicing (Kunze et al., 2000; Mittman et al., 1999). α1G is the best studied T-type Ca channel to date in this regard (Chemin et al., 2001). Fetal cardiac myocytes express α1G-d (Cribbs et al., 2001; α1G-bc by the nomenclature of Monteil et al., 2000a), whereas neuronal tissue preferentially expresses α1G-a or α1Ga-e, depending on the tissue (Dubin et al., 2000). These splice variants encompass the homologous repeat III-IV, as well as the II-III cytoplasmic linkers. From our modeling, the major differences appear to reside in the activation/deactivation gating transitions. It will therefore be interesting to use our model to account for phenotypic differences among the α1G splice variants. Future work is needed to determine whether there are specific amino acid sequences that are not conserved between the two isoforms (or splice variants) that are critical for these gating transitions.

APPENDIX

All of the rate constants on the top and bottom rows of the model, except for $k_{C3O} = k_{I3IO}$, have a voltage dependence (refer to Fig. 7). In the activation (forward) direction, the rate constants have the form:

$$\alpha(V) = \alpha \exp\{\delta\, q_i\, V/T\},$$

where $\alpha = k_{C1C2}, k_{C2C3}, k_{I1I2}, k_{I2I3}$. In the deactivation (back) direction, the rate constants have the form:

$$\beta(V) = \beta \exp\{-(1 - \delta)q_i\, V/T\},$$

where $\beta = k_{C2C1}, k_{C3C2}, k_{I2I1}, k_{I3I2}, k_{OC3}, k_{IOI3}$, the parameter T represents the thermal energy associated with room temperature in electron volts: $T =$ 25.4 mV; q_i, (i = 1, 2, 3) represents the gating charge (in units of fundamental charge) associated with the ith box in the model (numbered from left to right); and V is the membrane potential as determined by the voltage clamp command.

Assuming that the energy barrier associated with the transition between states is primarily associated with the membrane potential, the Boltzmann distribution implies that the ratio of the forward to back rate constants is given by:

$$\alpha(V)/\beta(V) = \alpha/\beta \exp\{q_i\, V/T\}$$

The parameter δ represents the fraction of the voltage dependence associated with the kinetics of the transition in the forward direction. For Box 3, parameter $\delta = 0$. For large depolarizations, the voltage dependence of the rate constants drives the equilibrium configuration toward the inactivated I_O state. In moving toward this equilibrium configuration, a certain portion of the channel proteins will pass through the open state O. Measurements of ionic current give a direct measure of the population of this open state. For resting (or hyperpolarized) membrane potentials, the equilibrium configuration is shifted to the left where an equilibrium is set up between the I_1 and C_1 states.

The kinetic scheme shown in Fig. 7 determines the transition matrix **A**, which is a function of the rate constants. It is this transition matrix **A(V)** that governs the time evolution of the state vector **X**:

$$\mathbf{X} = (I_O, I_3, I_2, I_1, C_1, C_2, C_3, O)$$

$$d\mathbf{X}/dt = \mathbf{AX}$$

During a voltage step, the equations are linear and the time dependence of the state vector is given by

$$\mathbf{X}(t) = \exp\{\mathbf{A}\, t\}\, \mathbf{X}(0)$$

To simulate the experimental measurement of gating current, we used a generalization of the matrix procedure used by Millonas and Hanck (1998). In place of their **Q** column vector, we constructed a gating charge matrix **S**. The ith row in the jth column in matrix **S** represents the effective amount of gating charge moved across the membrane in going from conformational state j to conformational state i. For example:

$$\mathbf{S}(I_1, I_O) = -(q_1 + q_2 + q_3)$$

$$\mathbf{S}(C_1, I_O) = -(q_1 + q_2 + q_3)$$

$$\mathbf{S}(I_O, I_1) = (q_1 + q_2 + q_3) = -\mathbf{S}(I_1, I_O)$$

Then assuming that the total population began in state j, the dot product of the jth column with the current state vector gives the amount of gating charge moved to reach the current distribution of conformational states. During a voltage step, the evolution equations are a linear system of equations so that the state vector $\mathbf{X}(t)$ is a superposition of solutions resulting from transitions beginning in each conformational state. As a result the total gating charge moved is a weighted sum of the gating charges moved during transitions from each conformational state according to the population of each state at $t = 0$. Turning these ideas into a matrix equation results in

$$Q = (\mathbf{S} \cdot \exp\{\mathbf{A}\, t\})\mathbf{X}(0)$$

$$I_Q = (\mathbf{S} \cdot \mathbf{A})\, \mathbf{X}(t),$$

where I_Q is the gating current and Q represents the total gating charge displaced during the voltage step. The dot operator (·) represents a dot product between the corresponding columns of the two matrices to produce a row vector. The final operation is a multiplication of the column vector on the right with this row vector to produce a scalar value. The second equation for the gating current comes from taking the time derivative of the first equation.

Because the dynamics of the gating currents occur on the order of a few milliseconds, the finite rise time of a voltage step becomes relatively important for these protocols. As a first step in checking the possible role

of a smoothed voltage step on a measured current trace, we modeled the voltage step as

$$V(t) = \Delta V[1 - \exp\{-k_{elec}\, t\}(1 + k_{elec}\, t)],$$

where ΔV is the voltage step, and $1/k_{elec}$ is an effective electronic time constant. At $t = 0$, both the applied voltage and the time derivative of the voltage are zero.

We thank Lindsay Burns for technical support and Dr. Leanne Cribbs for α1G.

This work was supported by AHA9806307 (D.B.) and National Institutes of Health HL63416 (J.S.).

REFERENCES

Aldrich, R. W., D. P. Corey, and C. F. Stevens. 1983. A reinterpretation of mammalian sodium channel gating based on single channel recording. *Nature.* 306:436–441.

Catterall, W. A. 1998. Structure and function of neuronal Ca^{2+} channels and their role in neurotransmitter release. *Cell Calcium.* 24:307–323.

Cha, A., P. C. Ruben, A. L., Jr.George, E. Fujimoto, and F. Bezanilla. 1999. Voltage sensors in domains III and IV, but not I and II, are immobilized by Na^+ channel fast inactivation. *Neuron.* 22:73–87.

Chemin, J., A. Monteil, E. Bourinet, J. Nargeot, and P. Lory. 2001. Alternatively Spliced α1G ($Ca_V3.1$) intracellular loops promote specific T-type Ca^{2+} channel gating properties. *Biophys. J.* 80:1238–1250.

Chen, C. F., and P. Hess. 1990. Mechanism of gating of T-type calcium channels. *J. Gen. Physiol.* 96:603–630.

Coulter, D. A., J. R. Huguenard, and D. A. Prince. 1989. Calcium currents in rat thalamocortical relay neurons: kinetic properties of the transient, low-threshold current. *J. Physiol. (Lond.).* 414:587–604.

Cribbs, L. L., J-H. Lee, J. Yang, J. Satin, Y. Zhang, A. Daud, J. Barclay, M. P. Williamson, M. Fox, M. Rees, and e. Perez-Reyes. 1998. Cloning and characterization of α1H from human heart, a member of the T-type calcium channel gene family. *Circ. Res.* 83:103–109.

Cribbs, L. L., B. L. Martin, E. A. Schroder, B. B. Keller, B. P. Delisle, and J. Satin. 2001. Identification of the T-type calcium channel ($Ca_V3.1d$) in developing mouse heart. *Circ. Res.* 88:403–407.

Droogmans, G., and B. Nilius. 1989. Kinetic properties of the cardiac t-type calcium channel in the guinea-pig. *J. Physiol. (Lond.).* 419: 627–650.

Dubin, A. E., J. Pyati, J. Y. Zhu, J. E. Galindo, R. Huvar, M. R. Jackson, M. G. Erlander, and R. W. Johnson. 2000. Novel isoform of a T-type α1G calcium channel isolated from human thalamus. *Biophys. J.* 78: 459a. (Abstr.)

Groome, J. R., E. Fujimoto, A. L. George, and P. C. Ruben. 1999. Differential effects of homologous S4 mutations in human skeletal muscle sodium channels on deactivation gating from open and inactivated states. *J. Physiol. (Lond.)* 516:687–698.

Hille, B. 2001. Ion Channels of Excitable Membranes, 3rd ed. Sinauer Associates, Sunderland, MA.

Huguenard, J. R. 1996. Low-threshold calcium currents in central nervous system neurons. *Annu.Rev. Physiol.* 58:329–348.

Huguenard, J. R., and D. A. Prince. 1994. Intrathalamic rhythmicity studied in vitro: nominal T-current modulation causes robust antioscillatory effects. *J. Neurosci.* 14:5485–5502.

Klockner, U., J. H. Lee, L. L. Cribbs, A. Daud, J. Hescheler, A. Pereverzev, E. Perez-Reyes, and T. Schneider. 1999. Comparison of the calcium currents induced by expression of three cloned a1-subunits, α1G, α1H and α1I of low-voltage-activated T-type calcium channels. *Eur. J. Neurosci.* 11:4171–4179.

Kozlov, A. S., F. McKenna, J. H. Lee, L. L. Cribbs, E. Perez-Reyes, A. Feltz, and R. C. Lambert. 1999. Distinct kinetics of cloned T-type calcium channels lead to differential calcium entry and frequency-dependence during mock action potentials. *Eur. J. Neurosci.* 11: 4149–4158.

Kunze, R., R. L. Martin, M. C. Emerick, W. S. Agnew, and D. A. Hanck. 2000. Kinetic differences in splice variants of the α1G T-type calcium channel. *Biophys. J.* 78:458a. (Abstr.)

Kuo, C-C., and B. P. Bean. 1994. Na^+ channels must deactivate to recover from inactivation. *Neuron.* 12:819–829.

Kuo, C. C., and S. Yang. 2001. Recovery from inactivation of t-type Ca^{2+} channels in rat thalamic neurons. *J. Neurosci.* 21:1884–1892.

Lee, J-H., J. C. Gomora, L. L. Cribbs, and E. Perez-Reyes. 1999. Nickel Block of Three Cloned T-type Calcium Channels: Low Concentrations Selectively Block α1H. *Biophysical Journal* 77:3034–3042.

Marksteiner, R., P. Schurr, S. Berjukow, E. Magreiter, E. Perez-Reyes, and S. Hering. 2001. Inactivation determinants in segment IIIS6 of CaV3.1. *J. Physiol.* 537:27–34.

Millonas, M., and D. A. Hanck. 1998. Nonequilibrium response spectroscopy and the molecular kinetics of proteins. *Phys. Rev. Lett.* 80: 401–404.

Mittman, S., J. Guo, and W. S. Agnew. 1999. Structure and alternative splicing of the gene encoding α1G, a human brain T calcium channel α1 subunit. *Neurosci. Lett.* 274:143–146.

Monteil, A., J. Chemin, E. Bourinet, G. Mennessier, P. Lory, and J. Nargeot. 2000a. Molecular and functional properties of the human α1G subunit that forms T-type calcium channels. *J. Biol. Chem.* 275: 6090–6100.

Monteil, A., J. Chemin, E. Bourinet, J. Nargeot, and P. Lory. 2000b. Identification of multiple human α1G isoforms of T-type calcium channels with distinct functional properties. *Biophys. J.* 78:199a. (Abstr.)

Patlak, J. 1991. Molecular kinetics of voltage-dependent Na^+ channels. *Physiol. Rev.* 71:1047–1083.

Perez-Reyes, E., L. L. Cribbs, A. Daud, A. E. Lacerda, J. Barclay, M. P. Williamson, M. Fox, M. Rees, and J-H. Lee. 1998. Molecular characterization of a neuronal low-voltage activated T-type calcium channel. *Nature.* 391:896–900.

Raman, I. M., and B. P. Bean. 1997. Resurgent sodium current and action potential formation in dissociated cerebellar Purkinje neurons. *J. Neurosci.* 17:4517–4526.

Satin, J., and L. L. Cribbs. 2000. Identification of a T-type calcium channel isoform in murine atrial myocytes (AT-1). *Circ. Res.* 86:636–642.

Serrano, J. R., E. Perez-Reyes, and S. W. Jones. 1999. State-dependent inactivation of the α1G T-type calcium channel. *J. Gen. Physiol.* 114: 185–201.

Staes, M., K. Talavera, N. Klugbauer, J. Prenen, L. Lacinova, G. Droogmans, F. Hofmann, and B. Nilius. 2001. The amino side of the C-terminus determines fast inactivation of the T-type calcium channel α1G. *J. Physiol. (Lond.).* 530:35–45.

Yarov-Yarovoy, V., J. Brown, E. M. Sharp, J. J. Clare, T. Scheuer, and W. A. Catterall. 2001. Molecular determinants of voltage-dependent gating and binding of pore-blocking drugs in transmembrane segment IIIS6 of the Na channel α-subunit. *J. Biol. Chem.* 276:20–27.

Zhang, Y., L. L. Cribbs, and J. Satin. 2000. Arachidonic acid modulation of α1H, a cloned human T-type calcium channel. *Am. J. Physiol. (Heart Circ. Physiol.).* 278:184–193.